EXTERNAL FACTORS INFLUENCE ON DEFECTS DETECTION BY SCANNING CONTACT POTENTIOMETRY

A.I. Alwaheba[1*], V.I. Surin[2]

[1]Jordan Atomic Energy Commission" Amman, Jordan
[2]National Research Nuclear University MEPhI, Moscow, Russia
*Corresponding author's e-mail address: anas.kloub@jaec.gov.jo

ABSTRACT

Scanning contact potentiometry (SCP) method was used to detect structural inhomogeneities in a welded joint under the application of heat and constant electric current. For this purpose, a special sample was prepared, welded by manual arc welding from two halves of X8CrNiTi18-10 (Chromium-Nickel-titanium stainless Steel) austenitic steel, each with dimensions of 200×110×13.5mm. After welding, welded sample was inspected using X-ray radiography. The sample was stored for five months at room temperature, and the sample surface was scanned using different scanning speed ranging from 0.36 to 1.8 mm/sec. It was found that when scanning speed was increased, the signal values remained the same. In another experiment, a constant electric current was passed through the sample from 0.01 to 0.1A. Applying current led to the excitation of weak structural inhomogeneities from the welding joint butt, although it was machined. While heat led to an increase in diagnostic signal amplitude.

KEYWORDS: Scanning contact potentiometry, welding joints, non-destructive testing, Chromium-Nickel-Titanium Stainless Steel.

1. INTRODUCTION

The contact between scanning sensor and the sample surface plays a vital role since the diagnostic signal is a result of low frequency waves of mechanical stresses emitted by defects in the welded joint. These mechanical waves are spontaneously generated by a rapid release of energy within a material due to changes in defect's local stress and strain fields in metals. Therefore, these waves can cause surface motion. These surface disturbances contain valuable information about location and characteristics of the defect [1-3]. On this basis, scanning contact potentiometry (SCP) had been developed. SCP is considered a reliable nondestructive testing method [4] where the relationship between deformational activity of the surface and electric properties of materials had been studied thoroughly by Surin et al [5,6].They found out that the growth of deformation subsequently lead to an increase in the number of spots of contact between the transducer and the sample surface, therefore resulting in a considerable increase in the amplitude of diagnostic signal. Moreover, SCP can detect the early stage formation and growth of embryonic fatigue cracks in metals [7].
The basis of SCP nondestructive testing is a simple physical approach, which considers the transducer-sample interface as a sensitive element. This approach allows us to measure the occurrence of an electrical signal at different structural levels and identify heterogeneities or structural failures at an early stage. For this purpose, the characteristic "structural signal level –SLS" is introduced as $SLS=|log|\Delta\varphi||$, where $\Delta\varphi$ is the measured value of the electric potential difference between transducer and sample surfaces [8].

In this case, it is important to clarify the concepts of electrical and mechanical contacts. When two metals come into contact, the two interacting surfaces are formed, and they act as effective barriers for conduction electrons. Forces arise between the atoms of these surfaces, leading to changes in their electron shells. The magnitude of interatomic forces depends on the gap between the surfaces [9,10].

When two metals are brought into contact, an exchange of electrons occurs between them, with electrons transferring from the metal with the smaller work function. The electro-potential method involves determining the signal value as the difference between the local work functions of the metals, divided by the electron charge [11].

The spectral density of the contact potential difference depends on the number of sources of deformation waves in the area of electrical contact, which are determined using harmonic analysis method [5]. The act of forming an inhomogeneous

Date of submission/acceptance: 31.05.2024/15.12.2024 http://doi.org/10.35219/awet.2024.05

surface deformation causes a jump in the amplitude of the electrical signal due to changes in the local work function and the conductivity of the contacting surfaces. The greater the number and area of contact spots between two metal surfaces, the higher the probability of electrons overcoming the dipole barrier.

The purpose of this study is to conduct SCP again and locate defects in an X8CrNiTi18-10 austenitic steel welded sample, consisting of two halves of 200×110×13.5mm plates, after five months of storing the sample at room temperature. Additionally, the influences of external factors (such as current and temperature) have been investigated. A constant current ranging from 0.01 to 0.1A was passed through the sample, and potentiograms were plotted and compared with those obtained directly after sample welding. Another objective was to examine how the scanning speed of the transducer on the welded sample surface affects the efficiency of detecting structural inhomogeneities compared to manual point-by-point scanning.

2. MATERIALS

Two plates of austenitic steel X8CrNiTi18-10 (Chromium-Nickel-Titanium steel), each with dimension of 200×110×13.5 mm, were welded together using manual arc welding. The welder intentionally created artificial discontinuities during the welding process.

X-ray radiographic testing of the welded seam was conducted using RAPAN M 200/100, SN 103326. Figure 1 displays a radiographic image of the weld seam, revealing deliberately inserted defects such as lack of root fusion (Da), incomplete fusion (Dc), edge offset or mismatches (Fd), cluster porosity (Aa), and Tungsten inclusions (Ca).

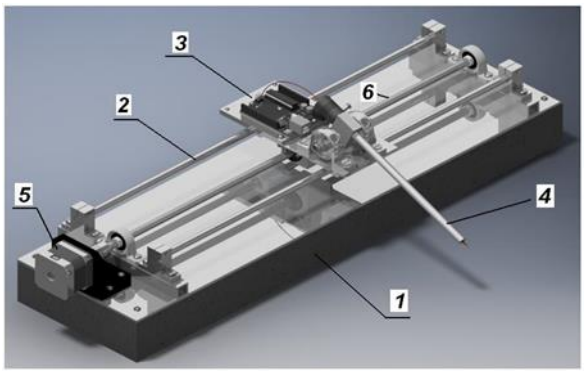

Fig. 1. Radiographic image of welding joint

In the weld seam axis, dark short lines are visible in the radiographic image. These lines appear more prominently in some areas than in others. These defects, indicated by the letters (Da), represent a lack of root fusion. Additionally, a thin dark line along the middle edge of the seam indicates incomplete fusion. The studied area, marked by arrows in the radiographic image, was later analysed using SCP.

Large clusters of pores are also evident in the radiographic image, notably under the sign "11" and in the central part. Another prominent defect, indicated by a relatively large dark spot almost in the middle of the seam, is the Worm-hole defect. This particular flaw was determined to be located 5mm from the sample surface using the ultrasonic method.

In the radiographic image, a Tungsten inclusion (Ca) stands out prominently as a light spot located to the left side of the Worm-hole defect.

SCP Electro-physical measurements were conducted using «ElphysLAB-IDS» system and LabVIEW software installed on an ASUS X554L laptop. The measurement technology is detailed in [8]. The studied area was divided into thirteen tracks, and potential values were recorded along these tracks. Surface scanning of the sample was carried out using the Spectroelph-FRR-450 device.

Spectroelph-FRR-450 device was utilized to conduct measurements on horizontally placed samples, featuring a measuring track of approximately 400mm. Sensor movement along the horizontal direction is facilitated by a stepper motor controlled by a PC via a USB serial interface (Fig.2).

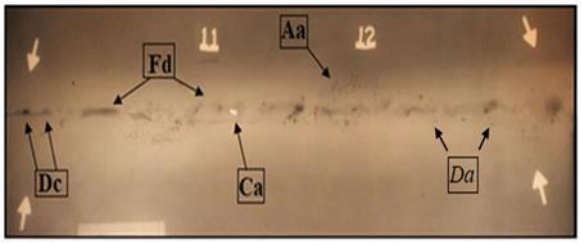

Fig. 2. Spectroelph-FRR-450 device:
1 - base; 2 - cylindrical guide; 3 - electronic unit and transducer holder; 4 - measuring rod (transducer); 5 - step motor; 6 - lead screw that converts rotary motion into linear motion

To enhance defect detection sensitivity, the weld bead was machined prior to measurement. The studied area was segmented into 13 tracks, with potential values recorded along each track. Six tracks were positioned to the left side of the welded joints relative to the axis of symmetry, and six to the right. Subsequently, scanning of the welding joint surface was conducted along these 13 tracks at varying speeds 0.36, 1.1, and 1.8mm/sec.

The signal, represented by the electric potential difference between the transducer and sample surface, is measured utilizing a transducer affixed to the end of the rod (4). This data is then transmitted via wire to the Agilent 34401A digital multimeter before being relayed to the PC.

During the electro-physical measurements, a steel transducer with a radius of 0.3mm was employed. The contacting angle between the sensor and the sample surface ranged from 45 to 60 degrees.

The diagnostic signal pertains to the strength of potential difference values generated between the transducer and the sample surface. These signals exhibit variation in amplitude. By establishing a specific threshold for the diagnostic signal, any signals surpassing that threshold will be filtered out, thereby enabling the detection of effective signals with lower amplitudes. These lower-amplitude signals contain valuable information about defects.

Potentiograms are constructed using various structural levels of the diagnostic signal (SLS). The analysis of potentiograms was conducted using MathCAD, which features a programmed amplitude filter for measuring signals based on the level of the diagnostic signal SLS. This filtering capability enables the categorization of signals by amplitude and the removal of those signal amplitudes exceeding the set level. Consequently, this allows for the examination of the distribution of electric potential at different scales.

The MathCAD program facilitates not only the linear scaling of individual defects, but also the adjustment of all images acquired for a specific SLS value. If fragments on potentiograms share identical amplitude values, they are assigned specific colours. Region with maximum signal amplitude, corresponding to a selected SLS value, are depicted in red and orange, while those with minimal positive or negative values are represented in blue and dark blue.

3. RESULTS AND DISCUSSION

3.1. Sensor Speed Influence

To investigate the impact of sensor speed on the efficiency of detecting structural inhomogeneities, a range of speeds were employed, spanning from 0.36 to 1.8mm/sec. Figure 3 illustrates the relationship between transducer scanning speed and the average value of the contact potential difference $\Delta\varphi$. The *x*-axis denotes the track number, while the *y*-axis represents $\Delta\varphi$ in Volts. Notably, the maximum and minimum speeds differ by a factor of five (0.36 to 1.8mm/sec), yet the average values of $\Delta\varphi$ across corresponding measuring tracks remain relatively consistent. This finding underscores the high reproducibility and sensitivity of SCP. Moreover, there is a discernible trend of increasing amplitude in the control signal with a rise in the number of measuring tracks. This can be attributed to the transducer approaching the active area (i.e., the region with inhomogeneities) and the surface of deformational activities as the number of measuring tracks increases.

The average values of $\Delta\varphi$ on tracks 11, 12, and 13 are nearly identical, as these tracks are situated far from the welding area (the welding seam axis corresponds to the 7th track). Additionally, it is apparent that structural inhomogeneities are present in the 10th measuring track, with the largest concentration of inhomogeneities occurring along the longitudinal axis of the welding seam (7th track). This observation is corroborated by the result of radiographic control.

It's worth noting that the average value of $\Delta\varphi$ is influenced not only by the quantity of inhomogeneities, but also by their specific structural type (e.g., root failure, Worm-hole defect, etc).

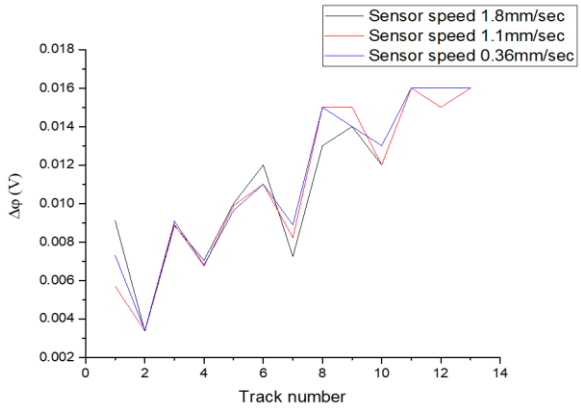

Fig. 3. Influence of transducer scanning speed along the measuring tracks on the average value of contact potential difference at room temperature

3.2. External Factors Influence on Structural Inhomogeneities

The investigation sought to elucidate the impact of temperature variations and constant electric currents on the intensity of emitted mechanical stress waves. Surface heating of the sample was accomplished utilizing the Lukey 702 heat gun for a duration of 10-15 minutes. Concurrently, a range of current values, specifically 0.01, 0.03, 0.05, 0.07 and 0.1A, were applied through the sample employing the Matrix model MPS-3005LK-3 device. Figure 4 shows the dependence of potential difference average value ($\Delta\varphi$) on current applied through the sample.

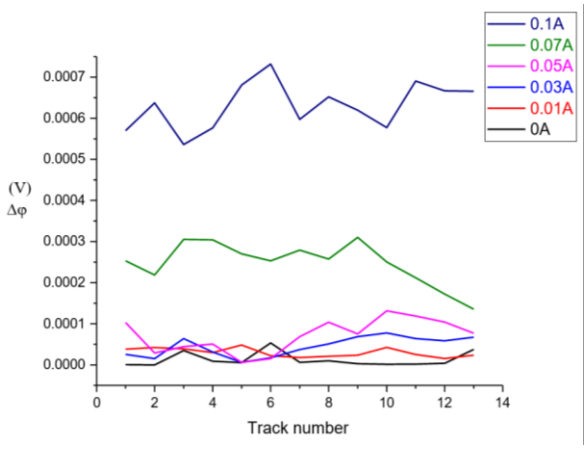

Fig. 4. The dependence of potential difference average value ($\Delta\varphi$) on current, applied through the sample

As the current passing through the sample intensifies, there is a corresponding gradual increase in the average potential difference ($\Delta\varphi$), as depicted in Figure 4, with the *x*-axis representing track number and the *y*-axis representing $\Delta\varphi$ in Volts. This behaviour of $\Delta\varphi$ signifies a concurrent elevation in the impact of the contact potential difference and a reduction in the work function of the electrons at the sample surface, attributable to the influence of surface current lines on the dipole barrier morphology. Consequently, alternations occur in the electric conductivity of the contact spots. Notably, at a current value of 0.1A, a pronounced decrease in $\Delta\varphi$ is observed in the 7th and 10th tracks, akin to the previous observation noted during changes in transducer speed.

At the upper portion of figure 5, the radiographic image of the welding seam is displayed. Within a white circle on the image, Tungsten inclusion (on the left) and the Worm-hole defect (on the right) are discernible. Beneath the radiographic image, potentiograms are depicted. The *x*-axis of the potentiogram represents the distance along the measuring tracks, with the maximum *x* value corresponding to the length of the weld joint (200mm).The *y*-axis denotes the track number. Images of all defects are discernible in the potentiogrammes. The resolution of defect images in the potentiograms is regulated by SLS level.

In figure 5a, evident observations include the lack of root penetration and edges offset. Figure 5b portrays an assortment of features including a Tungsten inclusion, pore clusters, Worm-hole defect, and additional inhomogeneities. The application of current and sample heating facilitates the identification of inadequate root fusion along the 7th track. This phenomenon is attributed to the activation of mechanical wave emission from defects and inhomogeneities induced by current and heat, as depicted in figure 5c, d, and e.

A comprehensive comparative analysis, conducted for identical levels of SLS, was undertaken to assess potentiograms obtained immediately after welding the sample and following five months of storage under ambient conditions. Analysis of the potentiograms indicates a reduction in the clarity of structural inhomogeneities images after the five-month period. This diminishment is attributed to the attenuation of the mechanical stress waves-emitting capacity of the structural inhomogeneities, resulting from the relaxation of residual stresses within the local volumes surrounding these defects.

Over time, the intensity of mechanical stress waves emission from the defects diminishes, consequently leading to the blurring of their images in the potentiograms.

Figure 6 illustrates potentiograms corresponding to SLS=5.699. Through analysis of the potentiograms provided for varying SLS values, the impact of aging on defect emission intensities becomes apparent.

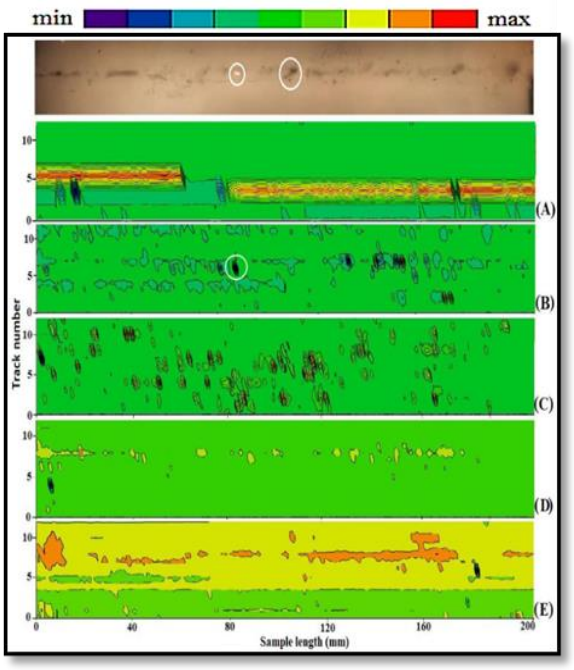

Fig. 5. Radiographic image (top) and potentiograms at SLS= 3.079: a) potentiogram immediately after welding; b) potentiogram after five months; c) potentiogram after heating sample surface up to 32°C; d) potentiogram when applying 0.03A current through the sample; e) potentiogram when applying 0.05A current through the sample

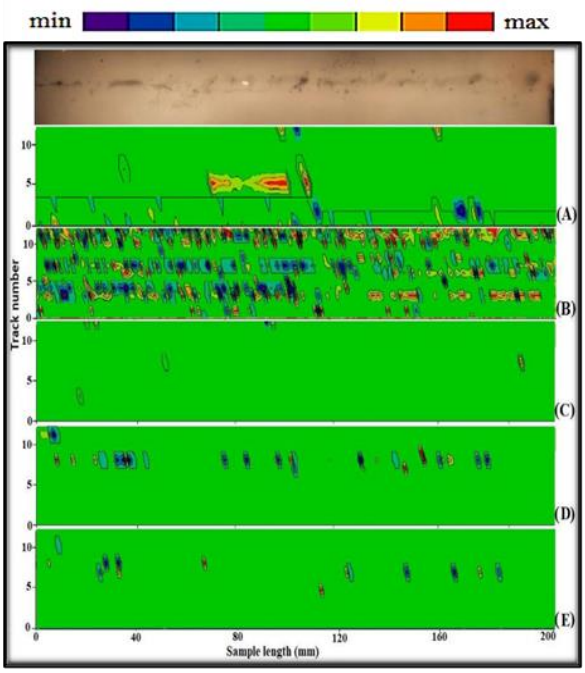

Fig. 6. Radiographic image (top) and potentiograms at SLS= 5.699: a) potentiogram immediately after welding; b) potentiogram after five months; c) potentiogram after heating sample surface up to 32ºC; d) potentiogram when applying 0.03A current through the sample; e) potentiogram when applying 0.05A current through the sample

When applying currents of 0.03 and 0.05A, extensive, broad bands become discernible on the potentiograms, particularly along tracks 6 and 7. These broad bands are recognized as indicative of lack of fusion. Notably, inhomogeneities on the potentiogram, sharing identical coloration, are situated at roughly equivalent depth.

The influence of heating on the value of $\Delta\varphi$ at a temperature of 39ºC was investigated. The average value of $\Delta\varphi$ for each track, as well as average values for 21ºC are depicted in figure 7. The *x*-axis denotes the track number, while the *y*-axis represents $\Delta\varphi$ in Volts. It's noteworthy that the temperature gradually decreased during the measurement process due to natural cooling to room temperature.

It's important to note the significant $\Delta\varphi$ jumps observed in the 4th and 10th measuring tracks in Figure 7. This behaviour of the signal is attributed to the variability in temperature regime during measurements and the occurrence of a thermoelectromotive force in the contact zone. Consequently, the presence of one of the largest inhomogeneities (edge offset) along the 10th measuring track yields a smaller signal in amplitude compared to approximately equivalents inhomogeneities situated along 4th and 5th tracks. The overall trend, characterized by a decrease in $\Delta\varphi$ with an increase in the track number, suggests that the sample undergoes cooling from the 5th to the 13th tracks. The lower values of the control signal for tracks 1, 2, 12 and 13 can be attributed to the presence of fewer structural inhomogeneities on these tracks, as well as their location outside the active zone (1st track). In contrast to the application of current, heating the sample surface results in a reduction in output operation on the 4th-5th and 10th tracks.

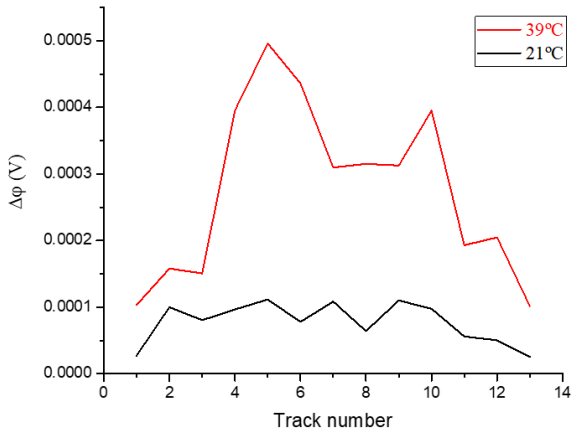

Fig. 7. Dependence of control signal $\Delta\varphi$ amplitude on the surface heating temperature.\

According to the work function theory of metals and alloys [12-13], a potential (dipole) barrier exists near the metal surface that prevents escape of electrons from the metal surface, impeding the escape of electrons from the metal surface. This barrier arises from the positive charge of ions, resulting from a deficiency of electrons in the near-surface region on the metal side, and, and the negative charge of the electron cloud near the metal surface. The thickness of the dipole barrier is exceedingly small, on the order of the electron wavelength, typically measured in Angstrom. To overcome this barrier, it is necessary to expend energy such that the kinetic energy of the electron surpasses the height of the potential well. At room temperature, the number of electrons possessing sufficient energy to overcome this barrier is negligible. However, upon heating the metal, the population of such electrons experiences a sharp increase.

4. CONCLUSIONS

The scanning contact potentiometry method was employed to investigate the influence of temperature and applied current on the efficacy of detecting structural inhomogeneities within a welded joint plate composed of two plates of austenitic steel X8CrNiTi18-10, each with dimensions of 200×110×13.5mm. The Effectiveness of detecting structural inhomogeneities was assessed by comparing potentiograms with results from radiographic control. Furthermore, a comparison was conducted between images of inhomogeneities in potentiograms obtained immediately after welding and those acquired after a five-month storage period under normal conditions. The identification of images in potentiograms yielded a satisfactory correspondence with images of the same defects observed in the radiographic control image.

An augmentation in the impact of the contact potential difference accompanies a concurrent decrease in the work function of the electron from the sample surface as the current increases from 0.01 to 0.1A. This phenomenon arises from the influence of surface current lines on the properties of the dipole barrier, including the barrier thickness and the concentration of electrons above the surface.

The observed nonlinearity of the control signal during the temperature relaxation to room temperature subsequent to heating the sample to 39°C is attributed to the fluctuating temperature conditions during the measurement process and the emergence of a thermoelectromotive force in the contact area. Notably, the most substantial amplitude jumps of the control signal were noted in the measuring tracks where the largest inhomogeneities are prevalent.

Additionally, it is noteworthy that the results obtained through SCP exhibit a high level of reproducibility when scanning the sample surface along thirteen measuring tracks at various transducer scanning speeds ranging from 0.36 to 1.8 mm/sec.

ACKNOWLEDGEMENTS

The authors would like to thank the welder Mr. Y.A. Kolykhalov in Tekhnoscan company for welding the

sample. This work was supported by Russian Foundation for Basic Research (RFBR) under grant 19-08-00266/19 from 10.01.2019.

REFERENCES

[1] **Wadley H. N. G., Scruby C. B., Speake J. H.,** *Acoustic emission for physical examination of metals*, International Metals Reviews, vol. 25, no. 1, 1980, pp. 41-64.
[2] **Eitzen D. G., Wadley H. N. G.,** *Acoustic emission: establishing the fundamentals*, Journal of research of the National Bureau of Standards, vol. 89, no. 1, 1984, pp. 75.
[3] **Mazille H., Rothea R.,** *The use of acoustic emission for the study and monitoring of localized corrosion phenomena*, Modelling Aqueous Corrosion: From Individual Pits to System Management, 1994, pp.165-174.
[4] **Surin V.,** *New potential for potentiometry*, Nuclear Engineering International, vol. 63, no. 765, 2018, pp. 30-32.
[5] **Ryabikovskaya E., Surin V.,** *Applying method of electrophysical diagnostics testing of uranium nitride under irradiation*, Energy Procedia, vol. 127, 2017, pp. 3-10.
[6] **Arefinkina S. E., Denisov R. A., Morozov A. A., Surin V. I.,** *Relationship between deformational activity of the surface and electric properties of materials*, Современные проблемы теории машин, vol. 4, no. 1, 2016, pp. 177-183.
[7] **Surin V. I., Polskij V. I., Osintsev A. V., Dzhumaev P. S.,** *Applying scanning contact potentiometry for monitoring incipient cracks in steels*, Russian Journal of Nondestructive Testing, vol. 55, 2019, pp. 59-67.
[8] **Alwaheba A. I., Surin V. I., Ivanova T. E., Ivanov O. V., Beketov V. G., Goshkoderov V. A.,** *Detection of defects in a welded joint by scanning contact potentiometry*, Nondestructive Testing and Evaluation, vol. 36, no. 3, 2021, pp. 261-277.
[9] **Ferrante J., and Smith J. R.** *Theory of metallic adhesion*, Physical Review B, vol. 19, no. 8, 1979, pp. 3911-3920.
[10] **Rose J. H., Ferrante J., Smith J. R.,** *Universal binding energy curves for metals and bimetallic interfaces*, Physical Review Letters, vol. 47, no. 9, 1981, pp. 675-678.
[11] **Blatt F. J., Schroeder P. A., Foiles C. L., Greig D.,** *The thermoelectric power of transition metals*, Thermoelectric Power of Metals, 1976, pp. 135-190.
[12] **Smith J. R.,** *Self-consistent many-electron theory of electron work functions and surface potential characteristics for selected metals*, Physical Review, vol. 181, no. 2, 1969, pp. 522-529.
[13] **Lang N. D., Kohn W.,** *Theory of metal surfaces: work function*, Physical Review B, vol. 3, no. 4, 1971, pp. 1215-1223.